Defect behavior during growth of heavily phosphorus-doped Czochralski silicon crystals. I. Experimental study EP

Masataka Hourai,[1] Yasuhito Narushima,[2] Kazuhisa Torigoe,[1,a] Naoya Nonaka,[1] Koutaro Koga,[1] Toshiaki Ono,[1] Hiroshi Horie,[1] and Koji Sueoka[3]

AFFILIATIONS

[1]Production and Technology Division, SUMCO Corporation, Imari-shi, Saga 849-4256, Japan
[2]Product & Technology Division, SUMCO TECHXIV Corporation, Omura-shi, Nagasaki 856-8555, Japan
[3]Department of Communication Engineering, Okayama Prefectural University, Soja-shi, Okayama 719-1197, Japan

Note: This paper is part of the special topic, Defects in Semiconductors 2024.
[a]Author to whom correspondence should be addressed: ktorigoe@sumcosi.com

ABSTRACT

This report (I) aims to investigate defect behavior during the growth of heavily phosphorus (P)-doped Czochralski silicon (HP-Cz-Si) crystals. The defects and P chemical states in as-grown crystals with a resistivity of 0.6 mΩ cm and the wafers annealed at around 600 °C were evaluated by transmission electron microscopy and hard x-ray electron spectroscopy (HAXPES). Micro-dislocation loops (MDLs) were observed in the bottom portion of the crystal, and larger stacking faults (SFs), including complex dislocation clusters, were observed in the middle portion. HAXPES revealed two different P states, P1 and P2. P1 was attributed to a substitutional P (P_s). The P2 present in as-grown crystals was found to be electrically active, while the newly formed P2 after annealing was electrically inactive, indicating that they are in different states. HAXPES evaluation of HP-Cz-Si after electron irradiation showed similar behavior to P2 after annealing, suggesting that P-vacancy (V) clusters are formed when the crystals are held at temperatures below 600 °C during crystal growth. Combining the experimental results with our theoretical analysis in the report (II) based on density functional theory calculations, we identified the following defect formation mechanisms. Interstitial P (P_i) atoms introduced at the melting point become supersaturated during cooling to 600 °C, and MDLs are generated by the aggregation of Si self-interstitials (Is) released through a position exchange from P_i to P_s. In crystal portions with a long residence time below 600 °C, supersaturated P_s transforms into P–V clusters, and Is generated simultaneously are absorbed by the MDLs, which grow into SFs containing dislocation clusters.

I. INTRODUCTION

Heavily phosphorus (P)-doped Czochralski-Si (HP-Cz-Si) crystals are widely used as substrates of n/n^{++} epitaxial (epi) wafers for low-voltage power MOSFETs, which are key parts for power supplies in information technology (IT) devices. Since the resistivity of the n^{++} substrates accounts for a large proportion of the on-resistance of power devices, there has been an increasing need to reduce the resistivity of the n^{++} substrates. Heavily arsenic (As)-doped Cz-Si crystals were conventionally used for such n^{++} substrates; however, it was difficult to lower the resistivity below 2 mΩ cm, so there has been a shift toward HP-Cz-Si crystals.[1]

Currently, the most advanced HP-Cz-Si crystals can be mass-produced with a low resistivity of 0.6 mΩ cm and a P concentration ([P]) up to 1.3×10^{20}/cm³, which is mainly constrained by constitutional supercooling.[2–4] However, in the epi-layer grown on the HP-Cz-Si substrates below 1 mΩ cm, epi-defects such as epi-stacking faults (SFs)[5] surrounded by {111} planes and dislocation pairs consisting of their diagonal ridges become apparent. In epi-layers grown on a 200 mm diameter HP-Cz-Si crystal substrate (resistivity: top ~0.9 mΩ cm, bottom ~0.6 mΩ cm), epi-SFs are frequent in the middle portion in the first half of the crystal and low in density in the bottom portion of the latter half. Each portion of

the crystal is held for a few hours at temperatures determined by its distance from the solid–liquid interface during the tailing process. In particular, the epi-SF density peaks in the middle portion, which is held near temperatures around 600 °C during the tailing process. Thus, the density of the epi-SFs in the epi-layer grown on the HP-Cz-Si substrates strongly depends on the resistivity as well as the thermal history of the crystal, suggesting that the origins of epi-defects are formed during crystal growth. However, the actual type and formation mechanism of these defects remain unknown.

Senda et al.[6] observed plate-like SiP[7] precipitates of 100–200 nm in as-grown HP-Cz-Si crystals with a resistivity of less than 1 mΩ cm. Zeng et al.[8,9] also reported the formation of oxygen precipitates from the heterogeneous nuclei of small SiP precipitates during the heat treatment of HP-Cz-Si crystals. Subsequently, Wu et al.[10] also reported that post-annealing of HP-Cz-Si crystals with a maximum [P] of 7.35×10^{19}/cm^3 and a minimum resistivity of 1.01 mΩ cm at 450–1050 °C resulted in the formation of SiP precipitates of various crystallographic morphologies depending on temperature. Meanwhile, a deactivation mechanism in heavily As- or P-doped layers formed by ion implantation or doped epitaxial growth[11] has long been discussed to address the need for extremely shallow and highly doped n^{++} regions in advanced device technologies. Nobili et al. demonstrated from a number of experiments that the formation of dopant precipitates such as SiAs[12,13] or SiP[14–17] is the main cause of the dopant deactivation in silicon. In addition, As-vacancy (V)[18–23] or P–V clusters,[24–26] referred to as E-centers, have also been under debate by many researchers from both experimental and theoretical aspects.

The purpose of this study is to experimentally investigate the defect formation behavior in HP-Cz-Si crystal growth with resistivities less than 1 mΩ cm. In addition, in our report (II),[27] we theoretically studied a reaction mechanism with respect to the experimental results of the present study using density functional theory (DFT) calculations.

II. EXPERIMENTAL

Several HP-Cz-Si crystals with a diameter of 200 mm and resistivities of ~0.9 mΩ cm (top) and ~0.6 mΩ cm (bottom) were grown under normal and modified growth conditions. Under the normal condition, crystals were grown in a mass-production manner as explained in Sec. I. Hereafter, we refer to them as crystals grown under the normal condition. In contrast, under the modified growth conditions, in order to promote defect formation reactions during crystal growth, the crystals were held for 10 h without growing immediately before or after the tailing process and then cooled rapidly after being detached from the Si melt. Hereafter, the crystals grown under these conditions are referred to as crystals with growth halting before or after the tailing process.

As-grown wafers were taken from the crystals, and defects were observed by a transmission electron microscope (TEM), a scanning transmission electron microscope (STEM), and energy dispersive x-ray spectroscopy (EDX). TEM observations were performed through the wafer cross section along the Si [110] direction using a Hitachi H-9000UHR-I with an acceleration voltage of 300 kV. The bulk defect density was determined by counting the number of defects within a total area of 2.54 μm × 1.62 μm × 10 fields of view or 2.20 μm × 2.10 μm × 8 fields of view using TEM,

with the average sample thickness being 300 nm. In the case of considerably low defect density, the number of fields of view was increased. To analyze the chemical composition of the defects, STEM-EDX elemental analysis mapping was performed using JEOL's JEM-ARM200F Dual-X with an acceleration voltage of 200 kV and an analysis beam spot size of 0.15 nm with atomic-level resolution. The P concentrations ([P]) in the wafers were measured using secondary ion mass spectrometry (SIMS) or an electron probe micro analyzer (EPMA). The carrier concentrations in the wafers were measured at room temperature by Hall effect measurement. In addition, the chemical bonding states of P were investigated by measuring the P_{1s} inner-shell photoelectron spectra using hard x-ray photoelectron spectroscopy (HAXPES, hv = 7.94 keV) at the beamlines BL46XU in SPring-8. The 0.6 mΩ cm samples ([P] = 1.3×10^{20}/cm^3) were scanned 70 times, and the 2.9 mΩ cm samples ([P] = 2.3×10^{19}/cm^3) were scanned 100 or 140 times.

To investigate the defect behavior at temperatures around 600 °C during crystal growth, wafers were taken from the bottom-most portion (~0.6 mΩ cm) of the crystals grown under the normal condition and divided into quarters along the ⟨110⟩ direction passing through the center of a single wafer. Each of the divided wafer was annealed in a nitrogen atmosphere at 520–700 °C for 5–20 h (short-time) and 520–600 °C for 10–30 days (long-time). Samples for TEM/STEM (size: ~10 × ~10 mm^2), SIMS/EPMA (~8 × ~8 mm^2), Hall effect (~8 × ~8 mm^2), and HAXPES (~2–3 × ~8 mm^2) were taken from a ~40 × ~40 mm^2 area at the center of these divided wafers. Additionally, HAXPES evaluation samples after annealing were prepared by chemically etching about 100 μm surface areas on one side to evaluate P states in the bulk. In addition, to introduce Vs into the wafers, HP-Cz-Si wafers with a resistivity of 2.9 mΩ cm ([P] = 2.3×10^{19}/cm^3) were irradiated with electron beams at doses of 1×10^{17}, 3×10^{17}, and 1.3×10^{18} e/cm^2 and evaluated by HAXPES and Hall effect measurement.

III. RESULTS AND DISCUSSION

A. Evaluation of defect behavior during crystal growth

1. TEM observation

Figures 1(a)–1(c) show the density-size distributions and TEM images of defects observed in as-grown wafers taken from the bottom 1 (solidification ratio ~60%) and 2 (~90%) portions of the crystal grown under the normal condition. The temperatures shown in Figs. 1(a) and 1(d) indicate the temperature ranges in which each crystal portion was held during the tailing process before it was cooled rapidly, where the temperature distribution during the growth of HP-Cz-Si crystals was obtained using the comprehensive heat transfer analysis software CGSim (Crystal Growth Simulator) code. In both portions, a high density of micro-dislocation loops (MDLs) smaller than 50 nm was observed with a peak density of around 15 nm as shown in Fig. 1(a). Figures 1(d)–1(f) also show the density-size distributions and TEM images of defects observed in the as-grown wafers taken from middle 1 (solidification ratio ~40%) and 2 (~50%) of the crystal grown under the normal condition. MDLs and SFs of around several hundred nm were observed with relatively low densities in both portions. Dislocation clusters were observed inside the SFs, in which several dislocations were highly tangled.

03 August 2024 06:47:31
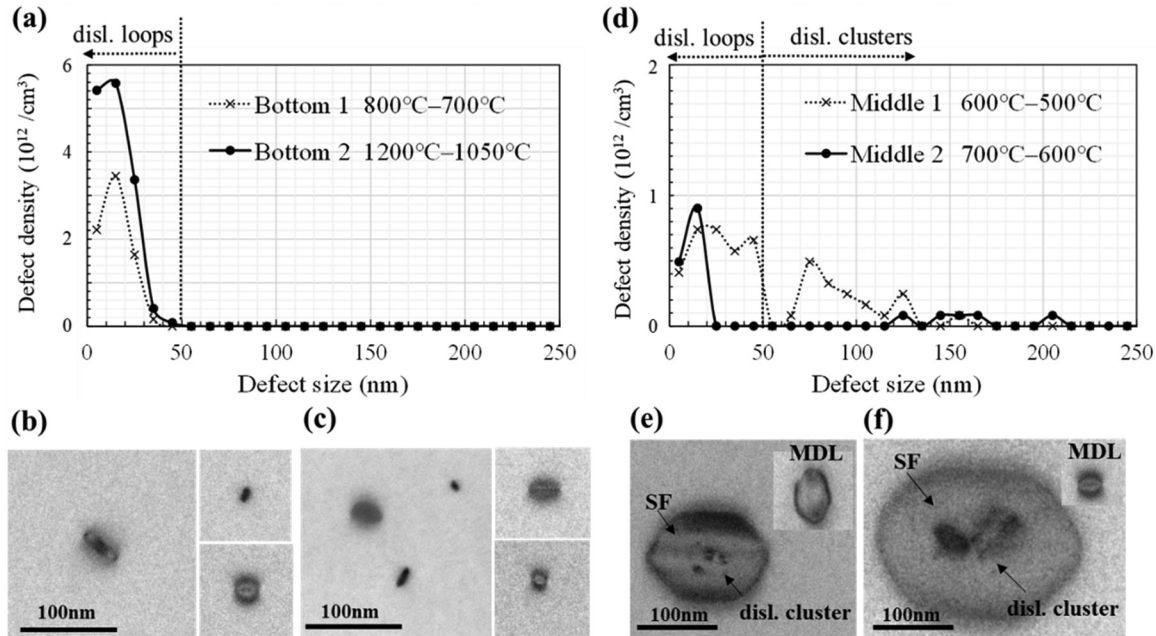
FIG. 1. Density-size distributions of defects observed in (a) bottom 1 (solidification ratio: ∼60%) and bottom 2 (∼90%), (d) middle 1 (∼40%) and middle 2 (∼50%) of heavily phosphorus (P)-doped Cz-Si (HP-Cz-Si) crystal (top: 0.9 mΩ cm, bottom: 0.6 mΩ cm), and TEM images of defects in (b) bottom 1, (c) bottom 2, (e) middle 1, and (f) middle 2. Temperatures in (a) and (d) are in the ranges held during the tailing process, and MDL and SF in (e) and (f) denote micro-dislocation loop and stacking fault, respectively. Detection limit of defect density in (a) and (d) is $8.2 \times 10^{10}/cm^3$.

Figure 2 shows the results of a fast Fourier transform (FFT) analysis for a high-resolution TEM lattice image of an MDL observed in the bottom portions. As shown in Fig. 2(e), the inverse FFT image from the (111) spots of the FFT pattern shown in Fig. 2(b) reveals that the defects are SFs with an extra {111} atomic layer. We also verified that these defects are Flank-type partial dislocations with a Burgers vector of $a/3\langle 111 \rangle$. Therefore, these defects are intrinsic SFs formed by an aggregation of supersaturated Si self-interstitials (Is) during crystal cooling.[28,29]

Our goal is to clarify the temperature ranges at which MDLs and SFs form in HP-Cz-Si crystals during crystal cooling and their dependency on the residence time or cooling rate at those temperatures. We also aim to investigate the generation mechanism of such interstitial-type defects. Toward this end, we conducted crystal growth halting experiments before and after the tailing process, making it possible to promote defect reactions that occur in specific temperature ranges during crystal growth.

Figure 3 shows the density-size distributions and TEM images of defects in as-grown wafers taken from the crystal with growth halting for 10 h before the tailing process, in which sample wafers were cut at multiple positions equally spaced 100 mm apart. In the bottom positions held at 945 and 778 °C, a high density of MDLs with sizes below 50 nm was observed, with a peak around 15 nm. These density-size distributions are similar to those in the bottom portions of the crystal grown under the normal condition shown in Fig. 1(a), and no significant differences were observed.

The crystals halted before the tailing process underwent polycrystallization due to dislocations, preventing the collection of samples

held at temperatures higher than 945 °C. However, the crystals halted after the tailing process grew without polycrystallization. This enabled us to evaluate the defects in the bottom portion held at approximately 1200–1050 °C for several hours during the tailing process, followed by a 10 h hold at about 1050 °C. MDLs with a density of $\sim4.5 \times 10^{12}/cm^3$ were also observed, with a similar density-size distribution as shown in Figs. 1(a) and 3 (778 and 945 °C). Thus, it can be concluded that the reactions for MDLs generation do not occur in the high-temperature range of about 1200–700 °C due to the insufficient supersaturation of Is. However, during the upward movement after crystal growth, these bottom portions typically passed through the intermediate temperature range below 700 °C at a quick cooling rate. This indicates that the supersaturation of Is becomes sufficiently high in the intermediate temperature range below 700 °C, leading to the generation of MDLs, regardless of the thermal history at higher temperatures during crystal growth.

Meanwhile, in the middle position held at 664 °C, significantly large defects (375–675 nm) were observed with a considerably lower density than those in the other positions. Furthermore, in the middle positions held at 565, 495, and 429 °C, MDLs smaller than 50 nm and medium-sized SFs smaller than 200 nm were observed to coexist, but their sizes tended to decrease with decreasing temperature. In particular, MDL growth was observed in the middle position held at 565 °C, and their density peak shifted to around 45 nm. In addition, medium-sized SFs (100–200 nm) appeared with very low density. In the middle position held at 495 °C, MDLs of about 5 nm were observed with higher density than those in the bottom positions held at 778 and 945 °C, and medium-sized SFs
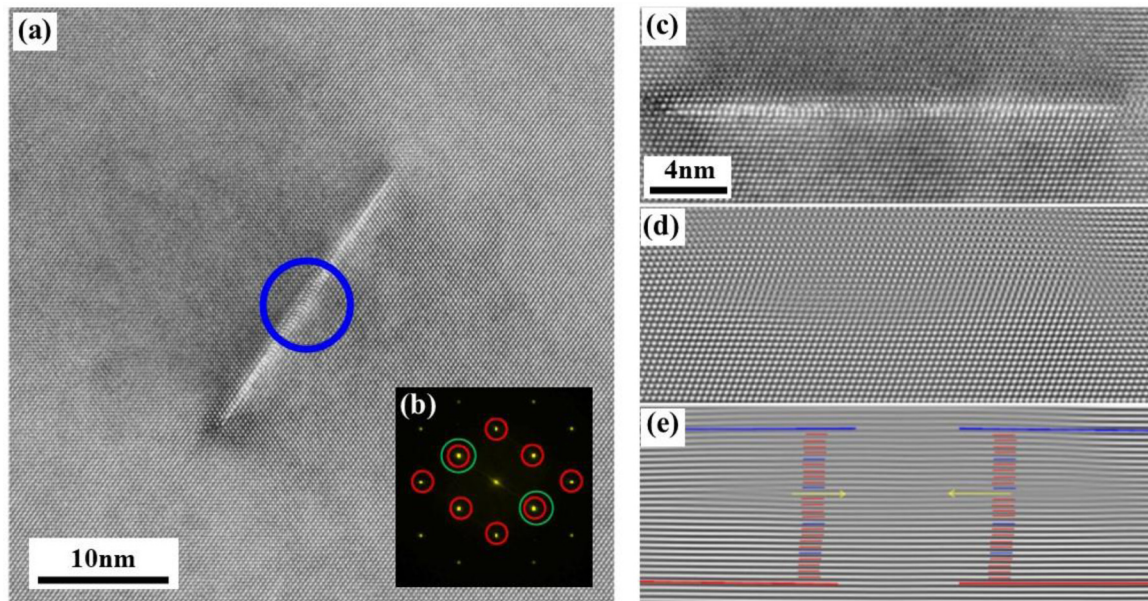
FIG. 2. Fast Fourier transform (FFT) analysis of the MDL in the bottom portion by TEM, (a) high-resolution TEM multiple beam interference image, accelerating voltage: 300 kV, (b) FFT pattern obtained from the area indicated by blue circle in (a), red circles: all spots, green circles: (111) spots normal to the defect, (c) high-resolution TEM multiple beam interference image, (d) inverse FFT (IFFT) image (all spots), (e) IFFT image (111), where yellow arrows indicate an interstitial-type dislocation loop.

(about 100 nm) with low density were also observed. In the middle position held at 429 °C, the density of the MDLs peaked at around 15 nm, which is similar to those in the bottom positions, but the defect size is more broadly distributed up to around 100 nm. In these middle portions held at 565–429 °C, the generation of new MDLs and the growth of pre-existing MDLs, which may be formed in the temperatures around 664 °C, proceeded simultaneously.

The above results demonstrated that MDLs and SFs coexist and that significant changes occur in the density-size distribution in various portions of the halted crystal, which were held at temperatures below 664 °C for 10 h and then rapidly cooled. As shown in Fig. 1(d), the coexistence of MDLs and SFs was also observed in the middle portions 1 and 2 of the crystal grown under the normal condition. These portions were held at about 700–600 °C and 600–500 °C, respectively, for several hours during the tailing process. The findings suggest that defects are hardly formed in the high-temperature range above 700 °C during the crystal cooling process. Instead, when Is become supersaturated at temperatures below 700 °C, interstitial-type defects such as MDLs and SFs are formed, and their density-size distribution changes depending on the residence time or cooling rate in the intermediate temperature range of approximately 700–500 °C.

As a mechanism for HP-Cz-Si to be I-dominant, Voronkov et al.[30] and Nakamura et al.[31] reported that the interstitial P (P_i) concentration increases with increasing [P], and the defect type changes from V to I when [P] exceeds 3.5×10^{19}/cm^3. In addition, in our report (II),[27] we clarified that about 1×10^{17}/cm^3 of P_i atoms are introduced during the solidification of HP-Cz-Si crystals when [P] is 1×10^{20}/cm^3. Table I shows the thermal equilibrium concentration and supersaturation of P_i obtained by first-principles calculations.[27] In HP-Cz-Si crystals with [P] $\sim 1 \times 10^{20}$/cm^3, Vs and Is are introduced at the melting point during solidification, and Vs remain near 1300 °C[32–34] due to their diffusion and recombination. P_i introduced at the melting point simultaneously becomes supersaturated at temperatures near 1100 °C. As a result, residual Vs are eliminated without generating voids through the reaction $P_i + V \leftrightarrows P_s$. As the temperature further decreases to 700 °C and below, the supersaturation of P_i significantly increases. Is released by the following reaction are also supersaturated:

$$P_i \leftrightarrows P_s + I. \qquad (1)$$

==Therefore, the aggregation of Is is believed to lead to the formation of MDLs.==

This phenomenon is similar to that in the formation of voids under a V-dominant condition or the formation of dislocation clusters under an I-dominant condition in P or B lightly doped Cz-Si crystal growth, where defect density and size are determined by the cooling rate in the temperature range in which defects are formed due to the aggregation of supersaturated point defects.[35,36] Furthermore, this is also similar to the phenomenon[37] where end-of-range (EOR) defects, which are formed on the crystal side of the amorphous/crystalline Si interface after ion implantation, coarsen and decrease in density depending on the annealing time due to the aggregation of supersaturated Is to form MDLs. Through kinetic analysis, this phenomenon has been found to occur via the Ostwald ripening growth mechanism.[37] Thus, the coarsening and decrease in defect density due to the residence time
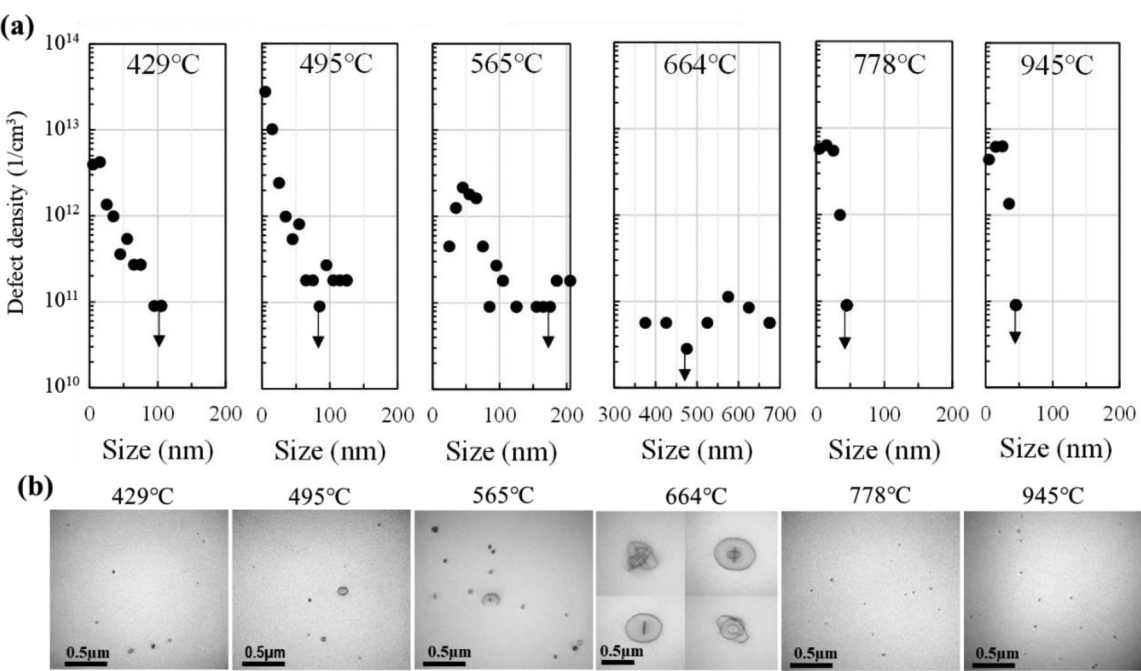
FIG. 3. (a) Density-size distributions and (b) TEM images of defects observed in various portions of the HP-Cz-Si crystal at temperatures during 10 h growth halting and immediately before rapid cooling without the tailing process. The arrows show the detection limits of defect density, and the tick marks on the vertical axis for each temperature in (a) are displayed on the leftmost side.

or cooling rate below 700 °C observed in the present study occurred most likely via the Ostwald ripening growth mechanism.

From the statistical data of SF densities and sizes obtained by TEM shown in Fig. 3, we estimated the amount of Is absorbed for the formation and growth of MDLs at each position, assuming that the SFs are disk-shaped atomic layers inserted in {111} planes. The amount of absorbed Is was derived using the formula absorbed $[I] = \Sigma 2\pi \cdot (Ln/2)^2 \cdot d\,(111)/V$, where Ln is the size (diameter) of the nth defect (SF) measured by TEM, $d\,(111)$ is the atomic density of the Si (111) plane (1.41×10^{15} atoms/cm^2), and V is the total

volume observed by TEM, calculated from $V = S \cdot D$. Here, S is the total field of view area and D is the average sample thickness in the observed area. Figure 4 shows the relationship between the amount of absorbed Is and the holding temperature of the crystal with growth halting before the tailing process. In the bottom positions held at 778 and 945 °C, about 1×10^{16}/cm^3 of Is were absorbed. In the middle portions held at 429 and 495 °C, a similar amount of

TABLE I. Thermal equilibrium concentration and supersaturation of P_i obtained by first-principles calculation.[27]

	$[P_i]^{mp} = 1 \times 10^{17}$/cm^3	
Temp (°C)	$[Pi]^{eq}$ (cm^{-3})	Supersaturation of P_i: $[P_i]^{mp}/[P_i]^{eq}$
1200	1.85×10^{17}	0.54
1100	7.78×10^{16}	1.29
1000	2.86×10^{16}	3.50
900	8.83×10^{15}	11.33
800	2.20×10^{15}	45.45
700	4.10×10^{14}	243.90
600	5.22×10^{13}	1 915.71
500	3.89×10^{12}	25 706.94
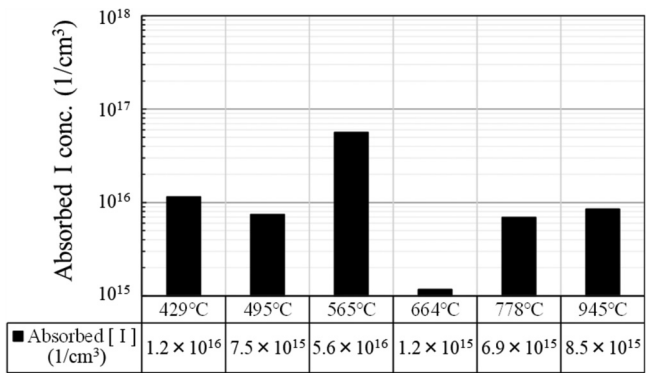
FIG. 4. Amount of Si self-interstitials (Is) absorbed for defect formation as a function of holding temperature in the crystal with 10 h growth halting and rapid cooling without the tailing process.
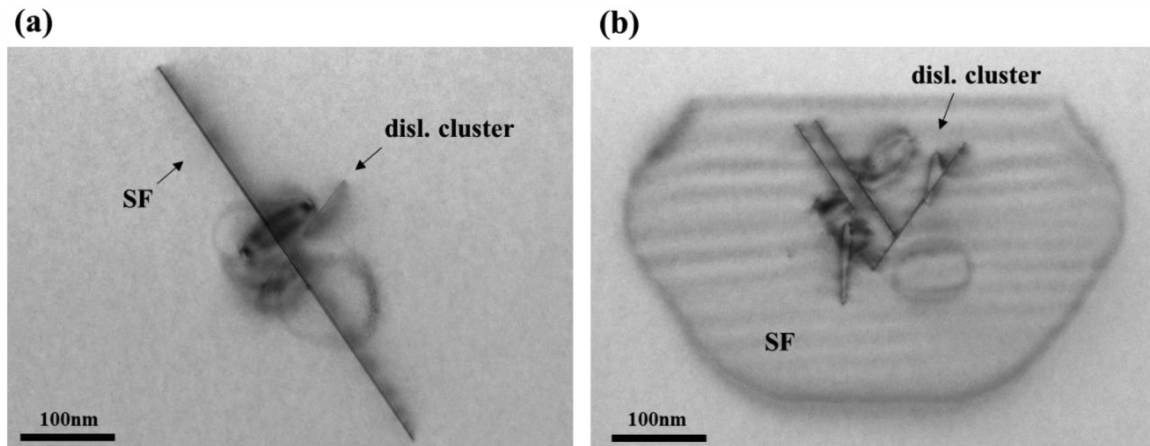
FIG. 5. TEM images of SFs observed in the middle portion (holding temperature: 700–600 °C) of the HP-Cz-Si crystal with 10 h growth halting and rapid cooling after the tailing process. (a) Linear and (b) hexagonal platelet SF including dislocation clusters.

Is (about 1×10^{16}/cm^3) was also absorbed, but in the middle position held at 565 °C, nearly 1×10^{17}/cm^3 was absorbed, which is almost one order of magnitude higher than those in the other positions. On the contrary, Is in the middle portion held at 664 °C was estimated to be about 1×10^{15}/cm^3, which was an order of magnitude lower than those in the other positions. In this region, it was difficult to accurately estimate the amount of Is due to the presence of highly tangled dislocation clusters inside the SFs, so the estimated value is expected to be lower than the actual value.

Figure 5 shows TEM images of defects observed in the middle portion of the crystal held at around 640 °C with growth halting for 10 h after the tailing process. Line-shaped dislocations and intricately entangled dislocation clusters can be clearly observed inside the SFs. Figures 5(a) and 5(b) show the same type of SFs on different {111} planes. The line-shaped dislocations inside the SF in Fig. 5(b) are regarded as immobilized stair-rod dislocations a/6 ⟨110⟩,[5,29,38] which are formed by a dislocation reaction due to the

intersection of SFs on different {111} planes. Such immobilized stair-rod dislocations are considered to be the origins of epi-SFs in the subsequent epitaxial process. Here, the TEM images in Fig. 5 are selected as typical examples showing the clear presence of stair-rod dislocations inside the SFs. These dislocations are commonly observed not only in crystals with growth halted before or after the tailing process but also in crystals grown normally, as shown in Fig. 1(f).

2. Analysis of P concentration distribution around defects

Figure 6 shows the results of STEM-EDX evaluation of the [P] distribution in the cross sections of SFs in the middle and bottom portions of the crystal with growth halting after the tailing process. These STEM images were also selected as typical examples showing the clear distribution of P atoms around the SFs, which is
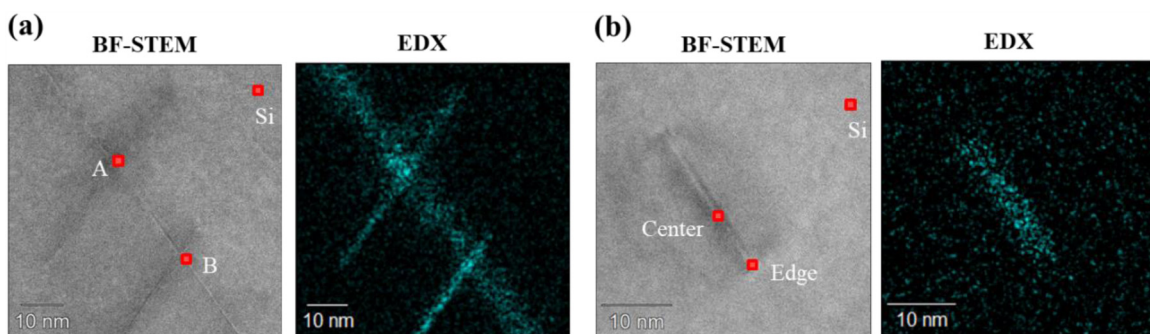
FIG. 6. Bright-field (BF)-STEM images and EDX phosphorus (P) concentration maps of defects observed in the HP-Cz-Si crystal with 10 h growth halting and rapid cooling after the tailing process. (a) SF including dislocation clusters in the middle portion (holding temperature: 600–500 °C), A and B indicate the intersections between the SF cross section and the linear dislocations. (b) MDL in the bottom portion (holding temperature: 1200–1050 °C).

TABLE II. Phosphorous concentration in defects measured by EDX. Red dots in Fig. 6 show the analysis points (— indicates that the value was under the detection limit).

Crystal portion (holding temp.)	Defect type	Analyzed position	[P] (at. %)
Middle (600–500 °C)	SF with dislocation clusters	A	6.93
		B	5.66
		Si matrix	—
Bottom (1200–1050 °C)	MDL	Center	1.19
		Edge	1.16
		Si matrix	—

commonly observed in crystals with growth halting before or after the tailing process as well as in crystals grown normally. The red dots in the figures are the locations where EDX spot analyses were performed, and the results are shown in Table II. As shown in Fig. 6, P atoms are diffusely distributed within a few nm from the SF planes. As shown in Table II, a relatively higher [P] was observed in the middle portion due to the diffusion of P atoms toward SFs during the holding at about 600–500 °C. In contrast, lower [P] was observed in the bottom portion where MDLs were formed during the rapid cooling in the upward movement following crystal growth.

Figure 7 shows the [P] distribution around an SF measured by a three-dimensional atom probe (3DAP) observed in the middle portion of the crystal under the normal growth condition. A [P] distribution of up to 5 at. % was observed in a roughly 5 nm width in front of and behind the SF plane. This is known as the Suzuki effect,[39,40] in which solid solution atoms segregate on SF planes due to the different chemical potentials of the solid solution atoms between in the crystal matrix and on the SF planes. Ohno et al.[41,42]

and Yamamoto et al.[43] also reported that P atoms segregate on the SF planes in Si crystals, resulting in a decrease in the energy of the SFs. Since the diffusivity of P_s is small near 600 °C, the P segregation can be attributed to the fast diffusion of P_i.[44–46] In our report (II),[27] we examined the segregation of P_i on SF planes using DFT model calculations and found that the energy is stabilized by about 0.8–2.0 eV per P_i atom as the P_i cluster grows on the SF plane, so many stable clusters of $(P_i)_2$–$(P_i)_7$ form quickly once one P_i atom is trapped on the SF.

3. Defect behavior during low-temperature annealing

To investigate the formation mechanism for the defects generated in the low temperature range of 500–700 °C, as-grown wafers with a resistivity of ∼0.6 mΩ cm were taken from the bottom-most portion of the crystal grown under the normal condition and annealed at low temperatures. Figure 8 shows changes in defects observed by TEM after as-grown and short-time annealing at 520–700 °C for 10 h and long-time annealing at 520–600 °C for 30 days. Starting from MDLs in the as-grown wafer shown in Fig. 8(a), the generation and growth of denser defects were found to depend on annealing temperature and time, as shown in Figs. 8(b) and 8(c). When the annealing time is extended at a constant temperature, the defect density remains consistent, but an increase in size is observed. Conversely, at a constant annealing time, increasing the temperature results in larger defect sizes but a tendency toward decreased density. These findings indicate that higher temperatures promote defect growth rates but suppress new defect generation. Further analysis should provide insight into the interaction between I_s and defects during crystal growth.

Figure 9(a) shows the amount of I_s absorbed for defect generation and growth during low-temperature annealing as functions of annealing time and temperature. Absorbed I_s clearly increased with
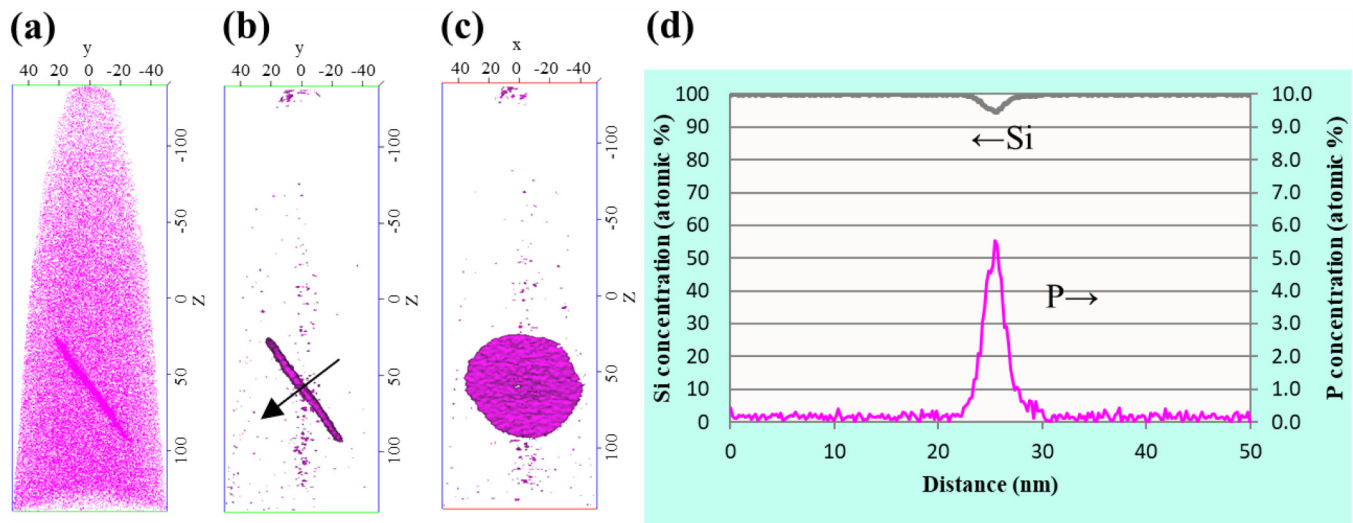
FIG. 7. Result of three-dimensional atom probe (3DAP) analysis of P concentration distribution of SF observed in the middle portion in the crystal grown under the normal condition. (a) P atom map, (b) 2% P iso-concentration plane, (c) 2% P iso-concentration plane rotated 90° from (b), (d) Si and P concentration profiles analyzed normal to the SF plane in the direction shown by the arrow in (b) (analysis range: φ50 × 50 nm).
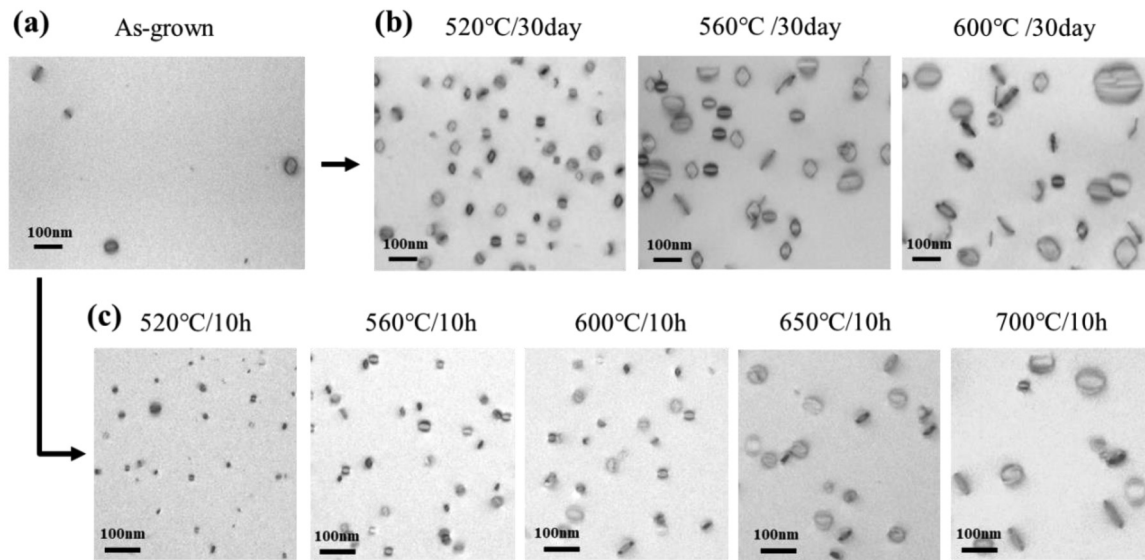
FIG. 8. TEM images of defects (a) in as-grown, (b) after long-time annealing at 520–600 °C/30 days, and (c) after short-time annealing at 520–700 °C/10 h for wafers taken from the bottom portion (∼0.6 mΩ cm) of the HP-Cz-Si crystal grown under the normal condition.

increasing annealing time and temperature. The Arrhenius plots of the absorption rate of Is are also shown in Fig. 9(b). The different activation energies above and below 600 °C suggest that the mechanism of I generation or absorption due to interactions with defects differs depending on temperature.

B. HAXPES evaluation of P chemical bonding states

1. States of P in as-grown HP-Cz-Si crystals

Figure 10 shows the P_{1s} inner-shell photoelectron spectra in HP-Cz-Si crystals with different resistivities. Two peaks, P1 and P2, were observed. The respective binding energies (E_b) were E_b (P1)

∼2144.6 eV and E_b (P2) ∼2143.6 eV, and the difference between the two binding energies $\Delta E_b = | E_b$ (P2)–E_b (P1) $| \sim$1.0 eV. The intensity of the spectrum decreased with increasing resistivity. Figure 11(a) shows the intensities of P1, P2, and P1 + P2, and the ratio of the intensity of P2 to P1 + P2 as a function of total [P] measured by SIMS. The intensity of P1 appears to be proportional to the total [P]. However, since the P2 ratios fluctuate by approximately 30%– 40% with respect to [P], the intensity of P2 is not considered to be proportional to [P].

Ike et al.[47] evaluated the P_{1s} inner-shell photoelectron spectra in the P-doped Ge epi-layer with [P] of 5×10^{19}/cm^3 by HAXPES and observed two peaks at E_b = 2143.1 and 2142.2 eV and
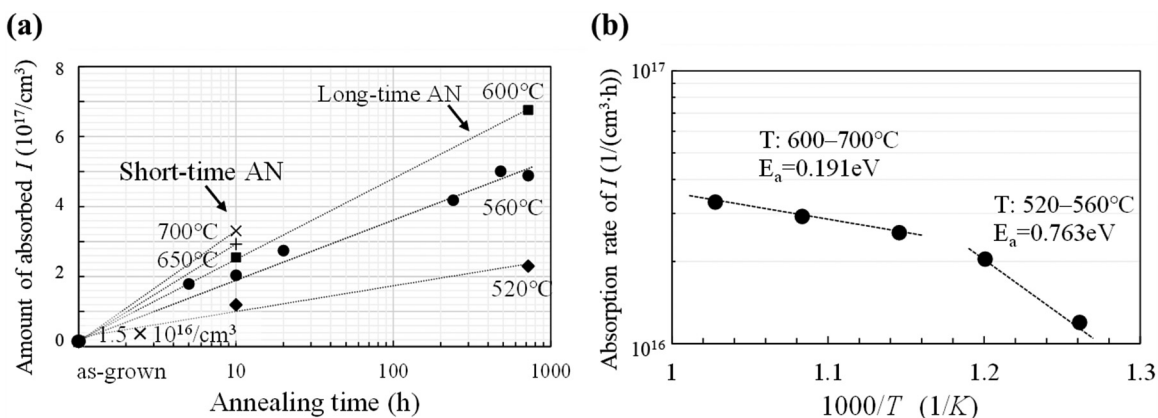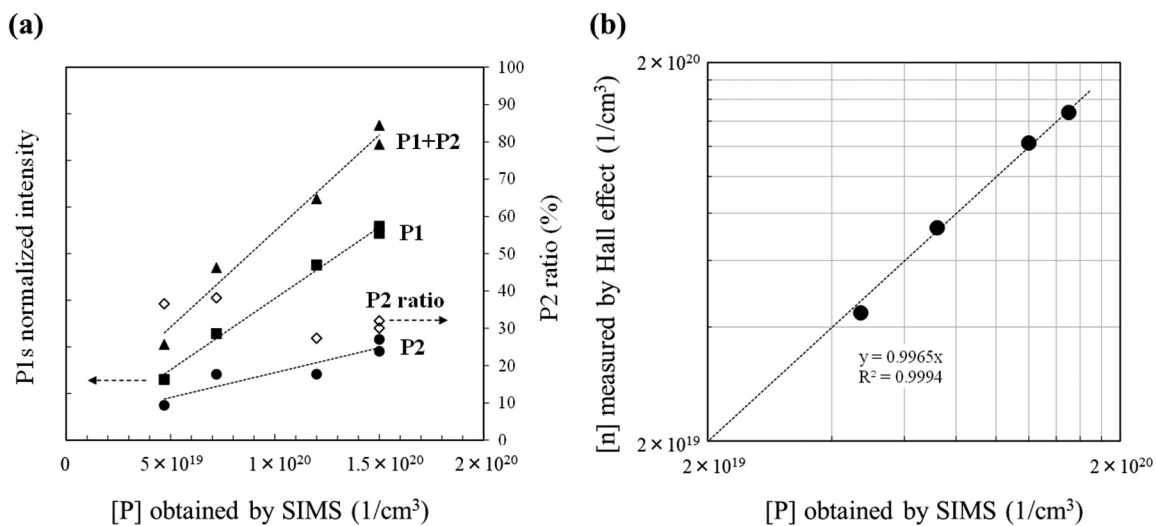

FIG. 9. (a) Amount of Is absorbed by defects during low-temperature annealing (AN stands for annealing). (b) Arrhenius plots of the absorption rate of Is.
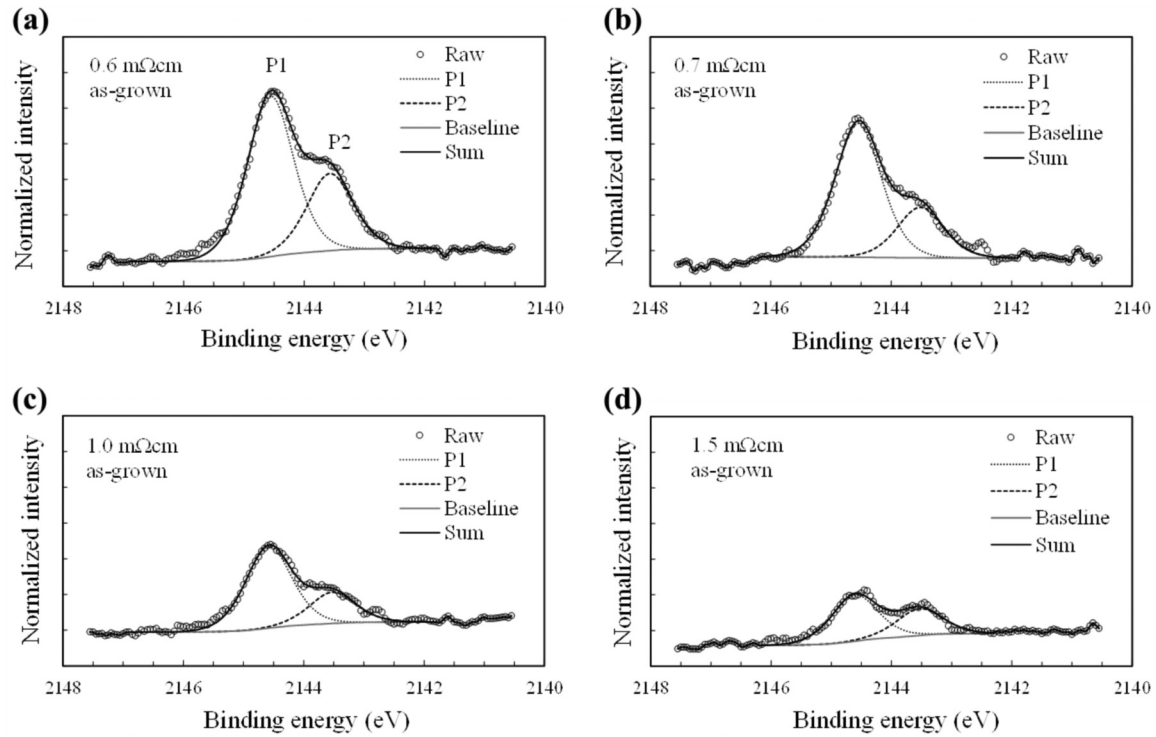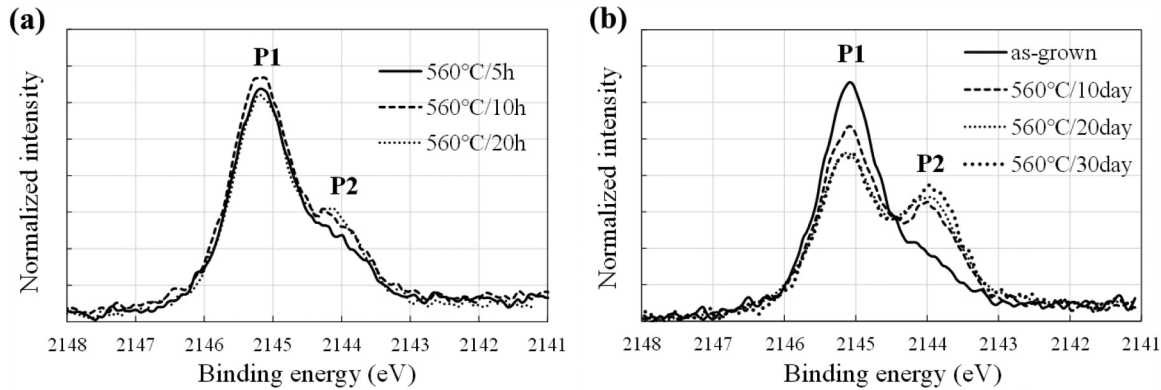
FIG. 10. P_{1s} inner-shell photoelectron spectra measured by HAXPES in as-grown HP-Cz-Si crystals with different resistivities, (a) 0.6, (b) 0.7, (c) 1.0, and (d) 1.5 mΩ cm.

FIG. 11. (a) P_{1s} normalized intensities of P1, P2, and P1 + P2, and ratios of P2 to P1 + P2 measured by HAXPES as a function of total [P] obtained by SIMS for HP-Cz-Si crystals with different resistivities, P1 and P2 indicate the peaks of the P_{1s} spectrum shown in Fig. 10(a). (b) Correlation between carrier concentration ([n]) determined by Hall effect measurement and total [P] obtained by SIMS in as-grown HP-Cz-Si crystals with different resistivities.

FIG. 12. Changes in P_{1s} inner-shell photoelectron spectra measured by HAXPES after low-temperature annealing. (a) Short-time annealing at 560 °C for 5–20h. (b) Long-time annealing at 560 °C for 10–30 days.

$\Delta E_b = 0.9$ eV. The peaks were identified as P^{1+} with a valence of +1 and P^0 with a valence of 0, respectively, i.e., the former as P_s and the latter as an electrically inactive P–V pair or cluster known as an E-center.[48–50] The similarity to our findings in this report (I) suggests that the main peak P1 observed in as-grown HP-Cz-Si crystals is a valence +1 P_s and the subpeak P2 is an electrically inactive P–V pair or cluster with a valence of 0. To verify that P2 in as-grown HP-Cz-Si crystals is electrically inactive, the Hall effect was used to measure the carrier concentration of samples with different resistivities shown in Fig. 10. Figure 11(b) shows the relationship between carrier concentration and total [P] measured by SIMS. Despite the large P2 ratio of 30%–40%, the carrier concentrations were almost identical to the total [P]. Therefore, we determined that P2 in as-grown HP-Cz-Si crystals is electrically active and in a different state from the P–V pairs or clusters.

2. State change of P in HP-Cz-Si crystal due to low-temperature annealing

Figure 12 shows the annealing time dependence of the P_{1s} inner-shell photoelectron spectra after annealing at 560 °C. Short-time annealing (5–20 h) resulted in little change, while long-time annealing of 10–30 days resulted in a decrease in P1 and an increase in P2. Figure 13 shows the carrier concentrations and resistivities after long-time annealing at 560 °C measured by the Hall effect. The carrier concentration was observed to decrease and resistivity increased as the annealing time increased. These results suggest that during long-time annealing at 560 °C, an inactive P2 of the order of 10^{19}/cm³ was newly generated from P1. These inactive P2, which are different from the active P2 in the as-grown state, will be referred to as P2′.

The table at the bottom of Fig. 13 shows [P], [P1], [P2], carrier concentration ([n]), resistivity, and the derived inactive P concentrations [P2′] and $[P]_{inactive}$ for as-grown and annealed samples, respectively. Here, [P1] and [P2] are the products of [P] measured by EPMA and the respective intensity ratios measured by HAXPES. The $[P]_{inactive}$ after annealing was calculated as $[P]_{An} - [n]$, where An indicates the state after annealing, and

$[P2′]_{An}$ was derived as follows. As shown in Fig. 11(b), since the P concentration in the as-grown state is almost equal to the carrier concentration, the P2 observed in the as-grown state is electrically active. In addition, assuming [P] = [P1] + [P2] for as-grown and annealed samples, as shown in Fig. 12(b), P1 decreases and P2 increases with long-time annealing, so it was hypothesized that P2′ after annealing is not a change from the active P2 existing in the as-grown state, but is generated by a change from P1. In this case, $[P]_{An} = [P1]_{An} + [P2]_{An} = [P1]_{An} + [P2]_{as-grown} + [P2′]_{An}$; then,

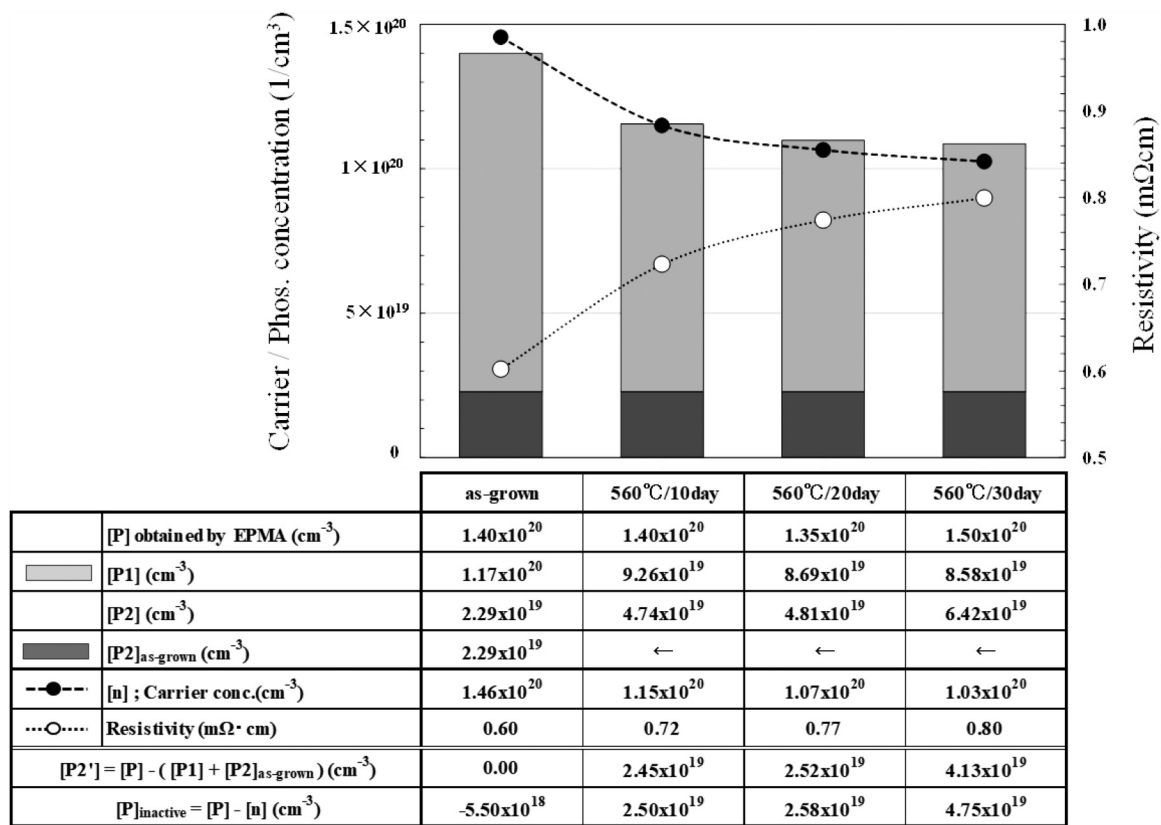$$[P2′]_{An} = [P]_{An} - \left([P1]_{An} + [P2]_{as-grown}\right) \qquad (2)$$

is derived.

[P2′] calculated from Eq. (2) is shown in the bar graph and table at the bottom of Fig. 13. Since the as-grown and annealed samples were divided from the same wafer, the arrow symbol in the column of $[P2]_{as-grown}$ in the table indicates the value of [P2] measured in the as-grown sample. As shown in Fig. 13, the carrier concentrations for as-grown and annealed samples are almost consistent with [P1] + [P2]$_{as-grown}$, and $[P]_{inactive}$ and [P2′] are relatively well-matched, supporting the above hypothesis. Thus, we concluded that the electrically active P2 existing in the as-grown state remains stable during low-temperature annealing, and the newly generated inactive P2′ in the order of 10^{19}/cm³ is formed by changes from P1.

3. State change of P in HP-Cz-Si crystals due to electron irradiation

To investigate the nature of P2′ newly formed by low-temperature annealing, electron irradiation was applied to HP-Cz-Si to introduce vacancies. Mäkinen et al.[51] performed electron irradiation to heavily P-doped Si with [P] = 1×10^{20}/cm³ at doses of 3×10^{16}, 3×10^{17}, and 3×10^{18} e/cm² and measured the positron lifetime using the positron annihilation method. The positron lifetime increased as the dose increased, indicating that P–V pairs are generated by electron irradiation. Figure 14 shows the P_{1s} inner-shell photoelectron spectra in the as-grown state and after

03 August 2024 06:47:31

		as-grown	560°C/10day	560°C/20day	560°C/30day
	[P] obtained by EPMA (cm^{-3})	1.40x10^{20}	1.40x10^{20}	1.35x10^{20}	1.50x10^{20}
	[P1] (cm^{-3})	1.17x10^{20}	9.26x10^{19}	8.69x10^{19}	8.58x10^{19}
	[P2] (cm^{-3})	2.29x10^{19}	4.74x10^{19}	4.81x10^{19}	6.42x10^{19}
	[P2]$_{as\text{-}grown}$ (cm^{-3})	2.29x10^{19}	←	←	←
	[n] ; Carrier conc.(cm^{-3})	1.46x10^{20}	1.15x10^{20}	1.07x10^{20}	1.03x10^{20}
	Resistivity (mΩ· cm)	0.60	0.72	0.77	0.80
	[P2'] = [P] − ([P1] + [P2]$_{as\text{-}grown}$) (cm^{-3})	0.00	2.45x10^{19}	2.52x10^{19}	4.13x10^{19}
	[P]$_{inactive}$ = [P] − [n] (cm^{-3})	−5.50x10^{18}	2.50x10^{19}	2.58x10^{19}	4.75x10^{19}

FIG. 13. Changes in carrier concentration and resistivity measured by Hall effect and in concentration of [P1] + [P2]$_{as\text{-}grown}$ measured by HAXPES after long-time annealing at 560 °C for 10–30 days. The arrow in the [P2]$_{as\text{-}grown}$ column in the table denotes the value of [P2] measured in the as-grown sample.

electron irradiation with a dose of 1.3×10^{18} e/cm^2 for HP-Cz-Si with a resistivity of ~2.9 mΩ cm and [P] ~2.3×10^{19}/cm^3. An increase in P2 ratio: P2/(P1 + P2) from about 17% to about 25% was observed after the electron irradiation dose of 1.3×10^{18} e/cm^2.

Figure 15 shows changes in carrier concentration determined by Hall effect measurements and total [P] measured by the EPMA before and after electron irradiation. The [P] did not change at all, while carrier concentration decreased with electron dose. We found
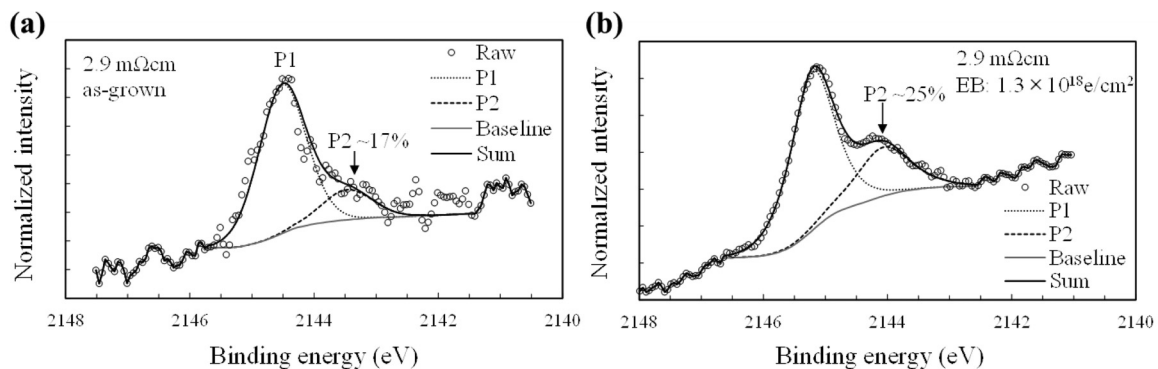
FIG. 14. P$_{1s}$ inner-shell photoelectron spectra by HAXPES of HP-Cz-Si crystal with a resistivity of 2.9 mΩ cm, (a) in as-grown sample and (b) after electron beam (EB) irradiation of 1.3×10^{18} e/cm^2.
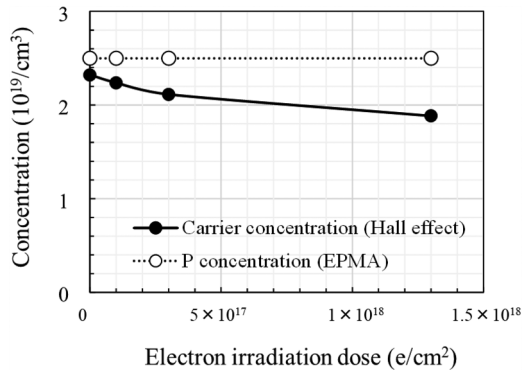
FIG. 15. P and carrier concentrations as a function of electron irradiation dose to HP-Cz-Si crystal with a resistivity of 2.9 mΩ cm.

that electron irradiation at the dose of 1.3×10^{18} e/cm^2 increased P2 ratio, by about 8%, which is equivalent to [P] × 0.08, approximately 1.8×10^{18}/cm^3 of electrically inactive P–V pairs or clusters as shown in Fig. 14. It also reduced the carrier concentration by about 4.4×10^{18}/cm^3 compared to before irradiation as shown in Fig. 15. In contrast, as shown in Fig. 13, P2′ increased by about 4.1×10^{19}/cm^3, and carrier concentration decreased by about 4.3×10^{19}/cm^3 after long-time annealing at 560 °C for 30 days. These results suggest that the long-time annealing at 560 °C produces electrically inactive P–V pairs or clusters in the order of 10^{19}/cm^3.

Ab initio total-energy calculations by Pandey *et al.*[18] showed that the formation of a new defect complex, a V surrounded by four As atoms, is responsible for the electrical deactivation and structural changes observed in x-ray absorption fine structure (XAFS) measurements when heavily As-doped Si is annealed. In other words, the As$_4$V complex is energetically more favorable than substitutional As or As$_4$Si coordination in Si and is neutral and electrically inactive. Rousseau *et al.*,[19] Pinacho *et al.*,[20,21] and Takamura *et al.*[24,25] reported that the ion implantation of high concentration As or P into Si substrates and low-temperature annealing at 500–700 °C induces the deactivation of the ion implanted n^{++} Si layer and accelerates the diffusion of the embedded B layer. They concluded that through the reactions As$_n$Si ↔ As$_n$V + I or P$_n$Si ↔ P$_n$V + I, As-V or P–V clusters were formed and Is were released.

Table III shows the binding energies of E_b(P1) and E_b(P2) and their differences of $\Delta E_b = |\, E_b(P2) - E_b(P1)\,|$ observed in various as-grown and processed HP-Cz-Si crystals. The as-grown crystals in Table III were grown under the normal condition and with growth halted for 10 h before and after the tailing process. Samples were taken from multiple portions of each crystal. The processed crystals consist of samples irradiated with electron beams and long-time annealed at 560 °C. The values in Table III represent the average and standard deviation of the measured values for each crystal sample. The ΔE_b for processed crystals were larger than 1.1 eV, while for all as-grown crystals, they were less than 1.1 eV. Therefore, the E_b of P2 or P2′ after electron irradiation or long-time annealing shifted slightly by about 0.1–0.2 eV lower than those of P2 in the as-grown crystals. These findings strongly suggest that the P2′ newly formed by long-time annealing at low temperatures below 600 °C is electrically inactive P–V clusters and in a different state from the electrically active P2 in as-grown crystals. However, the nature of electrically active P2 observed in the as-grown crystals, such as the chemical structure and determinants of concentration, could not be clarified in this study. Several candidate models for P clusters with a charge of +1 have been proposed in our report (II).[27] However, since the values of E_b and ΔE_b obtained from first-principles calculations are slightly different from the experimental values, a definitive model has not yet been determined and should be investigated in future research.

4. Another mechanism for Is generation below 600 °C

From the above experimental results, we arrived at the following reaction mechanism. That is, during the cooling process of the HP-Cz-Si crystal growth with [P] of about 1×10^{20}/cm^3, the P$_s$ in the middle portions held at temperatures below 600 °C becomes supersaturated,[44] and P–V clusters are formed in an amount undetectable by HAXPES through the following reaction:

$$nP_s \leftrightarrows (P_s)_nV + I \quad n = 1 - 4. \tag{3}$$

Accordingly, we concluded that reaction (3) is another mechanism for the generation of Is at temperatures lower than 600 °C, as suggested by the Arrhenius plots in Fig. 9(b). Additionally, if a crystal portion is held at temperatures above 600 °C, the concentration of Is supplied by mechanism (1) is limited to the concentration of P$_i$, which is at most 1×10^{17}/cm^3. However, if held at temperatures below 600 °C, a new Is generation mechanism (3)

	As-grown crystals			Processed crystals	
	Normally grown	Growth halted after tail	Growth halted before tail	Electron irradiated	Long-time annealed
E_b(P1) (eV)	2144.55 ± 0.01	2144.55 ± 0.01	2145.21 ± 0.01	2144.91 ± 0.42	2144.74 ± 0.39
E_b(P2) (eV)	2143.49 ± 0.07	2143.54 ± 0.01	2144.20 ± 0.03	2143.77 ± 0.43	2143.56 ± 0.41
ΔE_b (eV)	1.05 ± 0.05	1.01 ± 0.01	1.01 ± 0.04	1.14 ± 0.01	1.18 ± 0.03

03 August 2024 06:47:31

comes into play, allowing for the supply of a higher concentration of Is. This is believed to be the reason that the concentration of Is absorbed by defects in the portion held at 565 °C for 10 h, as shown in Fig. 4, is approximately an order of magnitude higher than those in portions held at temperatures above 600 °C.
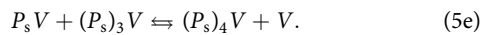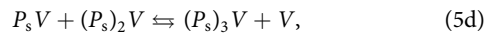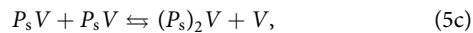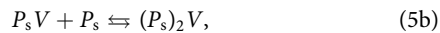
Furthermore, to decrease the supersaturation of Is, Is replace P_s with P_i through reaction (4),

$$I + P_s \leftrightharpoons P_i. \tag{4}$$

Such P_i atoms immediately become supersaturated at temperatures around 600 °C, but they diffuse quickly[14] and segregate on the surrounding SFs. The findings also suggest that the supersaturated Is and P_i atoms released in reactions (3) and (4) interact with the surrounding defects, which act as a sink to maintain their thermal equilibrium concentrations.

Similar to Pandey *et al.*[18] and Chen *et al.*,[26] in our report (II)[27] we found that because of the negative formation energy of −0.81 eV, $(P_s)_4 V$ at $n = 4$ is the most stable, and the equilibrium concentration balanced with given $[P_s]$ increases with decreasing temperature and reaches ~1×10^{19}/cm³ at around 600 °C for $[P_s]$ of 1×10^{20}/cm³. As shown in Fig. 12, no change in P2 was observed after short-time annealing, but after long-time annealing, P2′ of ~1×10^{19}/cm³, which is the equilibrium concentration of $(P_s)_4 V$ balanced with $[P_s]$ of ~1×10^{20}/cm³, was detected by HAXPES. This suggests that the formation of $(P_s)_4 V$ and Is through reaction (3) is the rate-limiting process for defect formation at temperatures below 600 °C in HP-Cz-Si crystal growth.

Chen *et al.*[26] proposed the following continuum models for the formation of $(P_s)_4 V$ clusters to explain the process of P deactivation based on *ab initio* calculations,

$$V + P_s \leftrightharpoons P_s V, \tag{5a}$$

$$P_s V + P_s \leftrightharpoons (P_s)_2 V, \tag{5b}$$

$$P_s V + P_s V \leftrightharpoons (P_s)_2 V + V, \tag{5c}$$

$$P_s V + (P_s)_2 V \leftrightharpoons (P_s)_3 V + V, \tag{5d}$$

$$P_s V + (P_s)_3 V \leftrightharpoons (P_s)_4 V + V. \tag{5e}$$

Here, V and $P_s V$ are assumed to be mobile species. When V encounters P_s, the mobile $P_s V$ pair is formed, and $P_s V$ forms $(P_s)_2 V$ with P_s or $P_s V$. $P_s V$ further migrates and reacts with $(P_s)_2 V$ and $(P_s)_3 V$ to form $(P_s)_3 V$ and $(P_s)_4 V$, respectively. The clustering reaction terminates at $(P_s)_4 V$ as the nearest neighbor sites of V are filled with P_s. Furthermore, when HP-Cz-Si with $[P] \sim 1 \times 10^{20}$/cm³ is held at temperatures below 600 °C, P_s becomes supersaturated, making the following reaction possible in parallel with (5a):

$$P_s \leftrightharpoons P_s V + I. \tag{5f}$$

Since MDL and SF defects serve as effective sinks for Is, the Is released by reaction (5f) are absorbed by the defects, leading to the continuous supply of $P_s V$. Therefore, if held at temperatures below 600 °C for a sufficient duration, the above series of clustering reactions will proceed until the thermal equilibrium concentration of $(P_s)_4 V \sim 1 \times 10^{19}$/cm³ at around 600 °C is reached.

IV. SUMMARY

Heavily phosphorus (P)-doped Czochralski silicon (HP-Cz-Si) crystals generate interstitial-type defects during crystal growth. Such defects induce epi-stacking faults in the epi-layer, degrading device characteristics. The purpose of this study was to experimentally investigate the defect behavior during the growth of HP-Cz-Si crystals. In our report (II),[27] the mechanism of defect formation was also studied theoretically by applying density functional theory (DFT) calculations with respect to the defect behavior studied in this report (I).

The defects and P chemical states in as-grown crystals with a low resistivity of 0.6 mΩ cm and wafers annealed at around 600 °C were evaluated by transmission electron microscopy and hard x-ray electron spectroscopy (HAXPES). Micro-dislocation loops (MDLs) were observed in the crystal bottom, and larger stacking faults (SFs), including complex dislocation clusters, were observed in the middle portion. HAXPES revealed two different P states, P1 and P2. P1 was attributed to a substitutional P (P_s). Meanwhile, although P2 existing in the as-grown crystal is electrically active, P2 which formed after long-time annealing below 600 °C was found to be inactive and was identified as P–vacancy (V) clusters.

Based on the experimental study in report (I) and the theoretical study in report (II), the formation of defects during the growth of HP-Cz-Si crystals at $[P] \sim 1 \times 10^{20}$/cm³ level can be summarized into the following four steps:

(1) During crystal solidification, Vs and Si self-interstitials (Is) are introduced, with a slight excess of Vs, and after their recombination, the Vs remain. The interstitial phosphorus (P_i) introduced simultaneously during solidification at a concentration of ~1×10^{17}/cm³ becomes supersaturated during crystal cooling. As a result, the remaining Vs are eliminated by the reaction $P_i + V \leftrightharpoons P_s$.

(2) As the crystal temperature decreases, P_i is further supersaturated, and the Is released by the reaction $P_i \leftrightharpoons P_s + I$ in the temperature range of about 700–600 °C also becomes supersaturated. This leads to the formation of MDLs through the aggregation of Is.

(3) Further lowering the crystal temperature below 600 °C increases the supersaturation of P_s, and Is newly released by the reaction $nP_s \leftrightharpoons (P_s)_n V + I$ are absorbed by MDLs, causing SFs to grow. Additionally, the P_i produced by the reaction $I + P_s \leftrightharpoons P_i$ segregates near surfaces of the SFs.

(4) Further absorption of Is leads to the generation of dislocation clusters inside the SFs. Some of them form stair-rod dislocations, which become the origins of epi-stacking faults during subsequent epitaxial growth.

AUTHOR DECLARATIONS
Conflict of Interest

The authors have no conflicts to disclose.

Author Contributions

Masataka Hourai: Conceptualization (lead); Formal analysis (lead); Investigation (lead); Methodology (lead); Project administration (lead); Validation (lead); Writing – original draft (lead); Writing – review & editing (lead). **Yasuhito Narushima:** Investigation (equal); Methodology (equal); Validation (equal). **Kazuhisa Torigoe:** Investigation (supporting); Methodology (supporting); Validation (equal); Writing – review & editing (supporting). **Naoya Nonaka:** Investigation (equal); Methodology (equal); Validation (equal). **Koutaro Koga:** Investigation (equal); Methodology (equal); Validation (equal). **Toshiaki Ono:** Investigation (equal); Methodology (equal); Validation (equal). **Hiroshi Horie:** Investigation (equal); Methodology (equal); Validation (equal). **Koji Sueoka:** Formal analysis (lead); Investigation (equal); Methodology (equal); Validation (equal).

DATA AVAILABILITY

The data that support the findings of this study are available within the article.

REFERENCES

[1] M. Porrini, J. Duchini, and A. Bazzali, Cryst. Res. Technol. **49**, 564 (2014).

[2] H. Kodera, Jpn. J. Appl. Phys., Part 1 **2**, 527 (1963).

[3] H. D. Chiou, J. Electrochem. Soc. **147**, 345 (2000).

[4] J. Friedricha, L. Stockmeiera, and G. Müllerb, Acta Phys. Pol. A **124**, 219 (2013).

[5] S. Mendelson, J. Appl. Phys. **35**, 1570 (1964).

[6] T. Senda, T. Ishikawa, H. Fujimori, H. Matsumura, S. Narimatsu, Y. Abe, and T. Horikawa, in *Extended Abstracts (The 78th JSAP Autumn Meeting, 2017)* (The Japan Society of Applied Physics, 2017), 7p-PB6-5 (in Japanese).

[7] S. Liang and R. Schmid-Fetzer, J. Phase Equilib. Diffus. **35**, 24 (2014).

[8] Y. Zeng, X. Ma, D. Tian, W. Wang, L. Gong, D. Yang, and D. Que, J. Appl. Phys. **105**, 093503 (2009).

[9] Y. Zeng, X. Ma, J. Chen, W. Song, W. Wang, L. Gong, D. Tian, and D. Yang, J. Appl. Phys. **111**, 033520 (2012).

[10] D. Wu, T. Zhao, B. Ye, H. Chen, X. Liang, S. Li, D. Tia, D. Yang, and X. Ma, J. Appl. Phys. **134**, 155701 (2023).

[11] C. H. Tsai, Y. H. Hsu, I. Santos, L. Pelaz, J. E. Kowalski, J. W. Liou, W. Y. Woon, and C. K. Lee, Mater. Sci. Semicond. Process. **127**, 105672 (2021).

[12] D. Nobili, A. Carabelas, G. Celotti, and S. Solmi, J. Electrochem. Soc. **130**, 922 (1983).

[13] D. Nobili, S. Solmi, M. Merli, and J. Shao, J. Electrochem. Soc. **146**, 4246 (1999).

[14] A. Armigliato, D. Nobili, M. Servidori, and S. Solmi, J. Appl. Phys. **47**, 5489 (1976).

[15] M. Finetti, P. Negrini, S. Solmi, and D. Nobili, J. Electrochem. Soc. **128**, 1313 (1981).

[16] D. Nobili, A. Armigliato, M. Finetti, and S. Solmi, J. Appl. Phys. **53**, 1484 (1982).

[17] S. Solmi, A. Parisini, R. Angelucci, A. Armigliato, D. Nobili, and L. Moro, Phys. Rev. B **53**, 7836 (1996).

[18] K. C. Pandey, A. Erbil, G. S. Cargill III, and R. F. Boehme, Phys. Rev. Lett. **61**, 1282 (1988).

[19] P. M. Rousseau, P. B. Griffin, W. T. Fang, and J. D. Plummer, J. Appl. Phys. **84**, 3593 (1998).

[20] R. Pinacho, M. Jaraiz, P. Castrillo, J. E. Rubio, I. Martin-Bragado, and J. Barbolla, Mater. Sci. Eng., B **114–115**, 135 (2004).

[21] R. Pinacho, M. Jaraiz, P. Castrillo, I. Martin-Bragado, J. E. Rubio, and J. Barbolla, Appl. Phys. Lett. **86**, 252103 (2005).

[22] F. F. Komarov, O. I. Velichko, V. A. Dobrushkin, and A. M. Mironov, Phys. Rev. B **74**, 035205 (2006).

[23] M. A. Berding, A. Sher, and M. van Schilfgaarde, Appl. Phys. Lett. **72**, 1492 (1998).

[24] Y. Takamura, S. H. Jain, P. B. Griffin, and J. D. Plummer, J. Appl. Phys. **92**, 230 (2002).

[25] Y. Takamura, P. B. Griffin, and J. D. Plummer, J. Appl. Phys. **92**, 235 (2002).

[26] R. Chen, B. Trzynadlowski, and S. T. Dunham, J. Appl. Phys. **115**, 054906 (2014).

[27] K. Sueoka, Y. Narushima, K. Koga, K. Torigoe, H. Horie, T. Ono, N. Nonaka, and M. Hourai, "Defect behavior during growth of heavily phosphorus doped Czochralski silicon crystals (II): Theoretical study."

[28] M. Okui, T. Tanaka, T. Kanda, and T. Ono, Oyo Buturi **66**, 707 (1997) (in Japanese).

[29] K. V. Ravi, *Imperfections and Impurities in Semiconductor Silicon* (Wiley, New York, 1981).

[30] V. Voronkov, R. Falster, M. Porrini, and J. Duchini, Phys. Status Solidi A **209**, 1898 (2012).

[31] K. Nakamura, S. Narimatsu, T. Senda, and S. Maeda, in *Extended Abstracts (The 80th JSAP Autumn Meeting, 2019)* (The Japan Society of Applied Physics, 2019), 18a-C212-5 (in Japanese).

[32] K. Nakamura, T. Saishoji, S. Togawa, and J. Tomioka, in *Proceedings of the Kazusa Akademia Park Forum on the Science and Technology of Silicon Materials* (Organizing Committee of Silicon Materials Science and Technology Forum, 1999), p. 116.

[33] M. Hourai, E. Asayama, H. Nishikawa, M. Nishimoto, T. Ono, and M. Okui, J. Electron. Mater. **49**, 5110 (2020).

[34] K. Sueoka, E. Kamiyama, and J. Vanhellemont, J. Appl. Phys. **114**, 153510 (2013).

[35] K. Nakamura, T. Saishoji, M. Nishimura, S. Togawa, and J. Tomioka, Proc. Kazusa Akad. Park Forum Sci. Technol. Silicon Mater. 197 (1997).

[36] M. Hourai, T. Nagsashima, E. Kajita, S. Miki, S. Sumita, M. Sano, and T. Shigematsu, J. Electrochem. Soc. **142**, 3193 (1995).

[37] C. Bonafos, D. Mathiot, and A. Claverie, J. Appl. Phys. **83**, 3008 (1998).

[38] J. Silcox and P. Hirsh, Philos. Mag. **4**, 72 (1959).

[39] H. Suzuki, J. Phys. Soc. Jpn. **17**, 322 (1962).

[40] J. F. Justo, A. Antonelli, T. M. Schmidt, and A. Fazzio, Physica B **273-274**, 473 (1999).

[41] Y. Ohno, T. Taishi, Y. Tokumoto, and I. Yonenaga, J. Appl. Phys. **108**, 073514 (2010).

[42] Y. Ohno, T. Shirakawa, T. Taishi, and I. Yonenaga, Appl. Phys. Lett. **95**, 091915 (2009).

[43] Y. Yamamoto, K. Togase, Y. Ohno, I. Yonenaga, and S. R. Nishitani, Jpn. J. Appl. Phys. **53**, 061302 (2014).

[44] B. Baccus, T. Wada, N. Shigyo, M. Norishima, H. Nakajima, K. Inoue, T. Iimura, and H. Iwai, IEEE Trans. Electron Devices **39**, 648 (1992).

[45] X.-Y. Liu, W. Windl, K. M. Beardmre, and M. P. Masquelier, Appl. Phys. Lett. **82**, 1839 (2003).

[46] P. Picheler, in *Intrinsic Point Defects, Impurities, and Their Diffusion in Silicon*, (Springer-Verlag Wien, New York, 2004), Chap. 5.

[47] S. Ike, W. Takeuchi, O. Nakatsuka, and S. Zaima, Semicond. Sci. Technol. **32**, 124001 (2017).

[48] S. K. Dhayalan, J. Kujala, J. J. Slotte, G. Pourtois, E. Simoen, E. Rosseel, A. Hikavyy, Y. Shimura, S. Iacovo, A. Stesmans, R. Loo, and W. Vandervorst, Appl. Phys. Lett. **108**, 082106 (2016).

[49] M. Yoshida, J. Appl. Phys. **48**, 2169 (1977).

[50] R. B. Fair and J. C. C. Tsai, J. Electrochem. Soc. **124**, 1107 (1977).

[51] J. Mäkinen, C. Corbel, P. Hautojärvi, P. Moser, and F. Pierre, Phys. Rev. B **39**, 10162 (1989).

03 August 2024 06:47:31